Local Conduction Velocity Mapping for Electrocardiographic Imaging

Corentin Dallet, Laura Bear, Josselin Duchateau, Mark Potse, Nejib Zemzemi, Valentin Meillet, Yves Coudière, Rémi Dubois

HAL Id: hal-01241751

https://inria.hal.science/hal-01241751

Submitted on 10 Dec 2015

Local Conduction Velocity Mapping for Electrocardiographic Imaging

Corentin Dallet[1,4], Laura Bear[1,4], Josselin Duchateau[1,4,5], Mark Potse[1,2],
Nejib Zemzemi[1,2], Valentin Meillet[1,5], Yves Coudière[1,2,3], Rémi Dubois[1,4]

[1]Electrophysiology and Heart Modeling Institute (IHU LIRYC), Bordeaux, France
[2]INRIA Bordeaux Sud-Ouest Carmen team, Bordeaux France
[3]IMB UMR CNRS 5251
[4]CRTCB INSERM U1045, Université de Bordeaux
[5]Hôpital Cardiologique du Haut Lévèque, CHU de Bordeaux, France

Abstract

Slow conduction is a well-known pro-arrhythmic feature for tachycardia and fibrillation. Cardiac conduction velocity (CV) mapping can be extremely helpful for investigating unusual activation patterns. Although methods have been developed to estimate velocity vector field, from ex-vivo preparations (e.g. from optical mapping recordings), the estimation from in-vivo electrograms (EGMs) remains challenging. This paper presents a new method specifically designed for EGMs reconstructed non-invasively from body surface potentials using electrocardiographic imaging (ECGi). The algorithm is based on cardiac activation maps and assumes either a linear or quadratic wavefront shape. The proposed methodology was performed on computed and experimental data for epicardial pacing on healthy tissue. The results were compared with reference velocity vector fields and evaluated by analyzing the errors of direction and speed. The outcomes indicate that a linear wavefront is the most suited for cardiac propagation in healthy tissue.

1. Introduction

The coordinated propagation of an electrical wavefront (WF) through the myocardium contributes to effective cardiac contraction in the healthy heart. This WF can slow down when it crosses pathological tissues, such as ischemia or scars. This activation latency allows the re-depolarization of healthy quiescent myocytes in neighbouring damaged tissue. This can cause an abnormal trigger leading to arrhythmias such as fibrillation or tachycardia. Therefore, estimating the velocity vector field to describe the local direction and speed of the propagating WF is a relevant tool to identify patients at risk of arrhythmia, and to localize pathological tissues for surgical treatments. To measure the WF pathway through the myocardium, electrograms (EGMs) are recorded across the ventricles.

For *ex-vivo* preparations, EGMs can either be recorded directly with electrodes applied to the heart, or derived from optical mapping. For these cases, accurate CV mapping methods have previously been developed [1]. For *in-vivo* experiments, EGMs can be recorded invasively using catheters or reconstructed non-invasively using electrocardiographic imaging (ECGi) from body surface potentials. While CV mapping algorithms have been developed, and are currently used clinically, for invasive recordings [2], ECGi reconstructions provide smoother EGMs. Hence, CV mapping has to be adapted to overcome these constraints.

In this study, we describe a novel method, specifically designed for EGMs reconstructed non-invasively, to estimate local epicardial velocity vector fields on the ventricles (Fig. 1). This tool uses the local activation time (AT) map, *i.e.* a geographic representation of the time when the electrical wavefront passes beneath each electrode. Then, it customizes a model linking the spatial coordinates of the electrodes to theirs ATs. It comes in two versions: a computationally efficient version which assumes a locally linear activation WF (CV1), and the second assuming a locally quadratic WF (CV2).
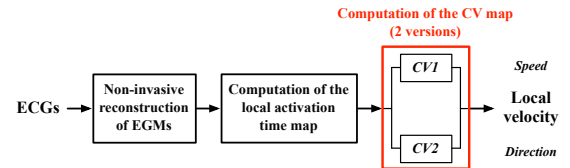

Figure 1. System overview: EGMs are reconstructed non-invasively using ECGi and ATs derived. A local region is then used to create the CV map assuming two activation WF shapes. This gives an estimate of the local velocity vector field containing information of speed and direction of the propagating electrical WF.

2. Methods

2.1. Forward problem

We used numerical simulations to construct reference data. The torso geometry was constructed from a CT scan of a 43-years-old woman. The geometry contained the body surface, the lungs, the bones, and the heart surface. We distinguished three different conductivity values: lungs, bones, and the rest of the tissue. In order to construct the body surface potentials, we used the bidomain model in the heart and the Laplace equation with heterogeneous conductivities in the torso. After adding different levels of noise on the body surface potentials (BSP), and without filtering, we solved the inverse problem based on an optimal control approach using a first order Tikhonov regularisation for both homogenous and heterogeneous torso conductivities.

2.2. Cardiac conduction velocity mapping

The local velocity vector, $\mathbf{V_i} = [V_i^X \, V_i^Y \, V_i^Z]$, at each electrode, i, is derived from a group of N neighbouring electrodes, for which the ATs $\tilde{T}_k$ and the 3-D coordinates $[X_k \, Y_k \, Z_k]$ are known, with $k \in [\![1\,;N]\!]$. The methodology is divided in three steps:

1) N electrodes $[X_k \, Y_k \, Z_k]$ are orthogonally projected into 2-D coordinates $[x_k \, y_k]$ using a singular value decomposition.
2) The local 2-D velocity vector $\mathbf{v_i} = [v_i^x \, v_i^y]$ at electrode i is calculated.
3) $\mathbf{v_i}$ is inversely projected into 3-D coordinates using the changing base found in 1, to get $\mathbf{V_i}$ on the original surface.
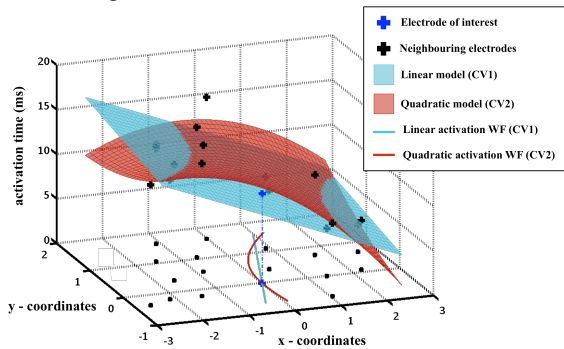

Figure 2. Representation of the locally linear (blue line and plane) and quadratic (red line and plane) activation WFs.

For step 2, the model linking the 2-D coordinates of each electrode to theirs ATs is customized in two ways. The first computationally efficient method (CV1) assumes a locally linear activation WF at electrode i (Fig. 2) defined as:

$$T(x,y) = a(x - x_i) + b(y - y_i) + c \qquad (1)$$

with $(a,b,c) \in \mathbb{R}^3$.

The second method (CV2), commonly used for *ex-vivo* preparations [1], assumes a locally quadratic electrical WF at electrode i (Fig. 2) defined as:

$$
\begin{aligned}
T(x,y) = a(x - x_i)^2 + \; b(y - y_i)^2 + \cdots \\
c(x - x_i)(y - y_i) + d(x - x_i) + e(y - y_i) + f
\end{aligned} \qquad (2)
$$

with $(a,b,c,d,e,f) \in \mathbb{R}^6$.

The model parameters $(a \ldots f)$ are calculated by minimizing the least square error between the reconstructed ATs, $\tilde{T}_k$ and those estimated with the model, $T(x_k, y_k)$:

$$\min_{a,b,c \ldots} \sum_{k=1}^{N} \left(T(x_k, y_k) - \tilde{T}_k \right)^2 \qquad (3)$$

$\mathbf{v_i}$ can then be calculated using the spatial gradient of $T(x,y)$ at the 2-D coordinates $[x_i \, y_i]$ of the electrode of interest i:

$$\mathbf{v_i} = \left. \frac{\nabla T(x,y)}{\|\nabla T(x,y)\|^2} \right|_{(x=x_i \; y=y_i)} \qquad (4)$$

with $\|\cdot\|$, the Euclidian norm.

2.3. Databases

Simulated Data

Propagating action potentials (APs) were computed with a mono-domain reaction-diffusion model on a finite-difference mesh with 0.2mm resolution. The transmembrane ionic currents were computed with the TNNP model [3], using different parameter values for the left and right ventricle and for the subendocardial, mid-myocardial, and epicardial layers. The simulated transmembrane currents were injected in a bi-domain torso model at 1mm resolution to compute the extracellular potential field, for each millisecond of simulated time. In this study, potentials extracted from 252 surface "electrode" sites were used as input for ECGi applying the MFS [4], and potentials extracted from 1629 epicardial points were used as validation data. The heart and torso models included anisotropic myocardium with transmural fiber rotation. The torso model had an anisotropic skeletal muscle layer. Simulations were performed with the propag-5 software [5] and run on a BlueGene/Q supercomputer operated by IDRIS (France).

In-situ Recordings

The methods were also evaluated using an *in-vivo* data set, obtained from an anaesthetized, closed-chest, pig [6]. Electrical signals were recorded simultaneously i) on the ventricular epicardium using a custom-made elastic sock consisting of 239 unipolar electrodes (5-10 mm spacing) and ii) across the thorax using flexible electrodes strips

(BioSemi, the Netherlands), containing 170 electrodes (30-45 mm spacing). Recordings were made during 10 different epicardial pacing sequences. Post-mortem MRI was used to construct a subject specific geometry, with MRI contrast markers to localize sock and strip electrodes. In this study, epicardial EGMs were reconstructed at the 239 sock electrode locations using ECGi and applying the MFS [4].

2.4.   Validation

As the velocity vectors contain information about the speed and direction of a propagating WF, both angle (5) and speed (6) errors are computed. For this, the CV1 and CV2 estimated velocity vectors $\mathbf{V_i^{CV1,2}}$ were compared to a gold standard (GS) $\mathbf{V_i^{GS}}$ for each electrode i

$$\theta_{err}^i = \left| \cos^{-1} \left(\frac{\langle \mathbf{V_i^{GS}} | \mathbf{V_i^{CV1,2}} \rangle}{\|\mathbf{V_i^{GS}}\| \times \|\mathbf{V_i^{CV1,2}}\|} \right) \right| \tag{5}$$

with $\langle \cdot | \cdot \rangle$, the scalar product.

$$s_{err}^i = \|\mathbf{V_i^{CV1,2}}\| - \|\mathbf{V_i^{GS}}\| \tag{6}$$

For the simulated data, the gold standard vector field $\mathbf{V_i^{GS}}$ was computed directly from APs; for the *in-vivo* data it was estimated from the recorded epicardial EGMs. Outlier values were removed from the analysis in accordance to the Tukey's statistics.

3.   Results

CV1 and CV2 were performed on each dataset and analysed. Table 1 displays the overall angle θ_{err} and speed s_{err} error values:

	Simulated model		Experimental model	
	CV1	CV2	CV1	CV2
θ_{err} (°)				
Median	22.94	23.11	27.74	33.17
1st quartile	11.52	11.50	13.05	15.22
3rd quartile	41.79	41.88	51.98	68.29
s_{err} (m/s)				
Median	0.49	0.50	1.24	1.32
1st quartile	0.17	0.17	0.47	0.51
3rd quartile	1.51	1.55	2.53	2.72

Table 1. CV1 versus CV2 angle (θ_{err}) and speed (s_{err}) errors.

(a) RV   *(b) RV*
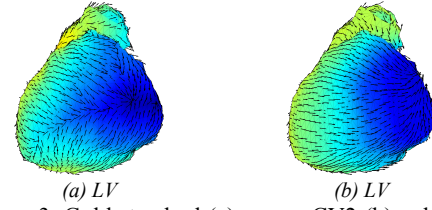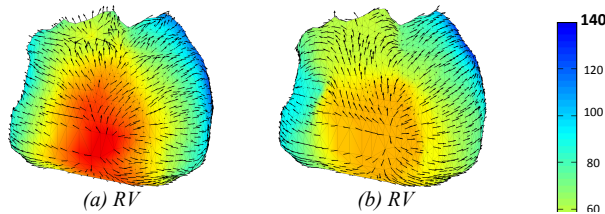

(a) LV   *(b) LV*

Figure 3. Gold standard (a) versus CV2 (b) velocity vectors for the simulated data. The onset of activation (red) is on the RV, the termination (blue) on the LV.

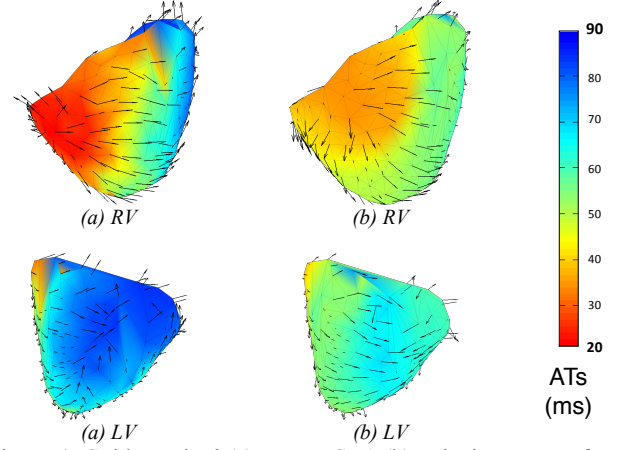*(a) RV*   *(b) RV*

(a) LV   *(b) LV*

Figure 4. Gold standard (a) versus CV1 (b) velocity vectors for the pig data. The onset of activation (red) is on the RV, the termination (blue) on the LV.

Fig. 3 and 4 show AT maps and the velocity vector fields for reference and non-invasive reconstructions. Fig. 3 displays the results from the realistic heart model for a RV freewall pacing sequence and Fig. 4 shows those for *in-vivo* data for a RV epicardial pacing sequence. Angle and speed errors for the above sequences are displayed on 3-D meshes in Fig. 5 and 6 respectively.
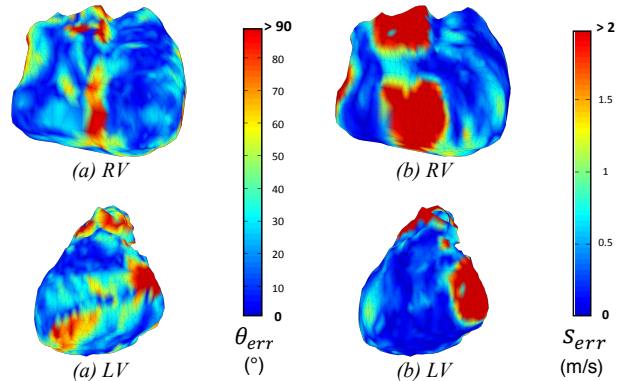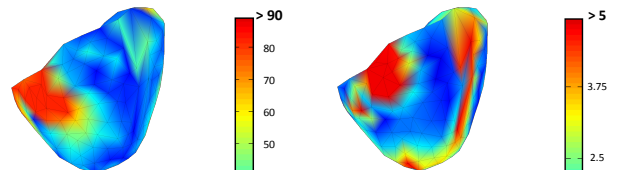

(a) RV   *(b) RV*

(a) LV   *(b) LV*

Figure 5. Angle (a) and speed (b) errors on the ventricles, performing CV2 on the simulated data.

θ_{error} s_{erro}

(a) RV　　　　　　　*(b) RV*
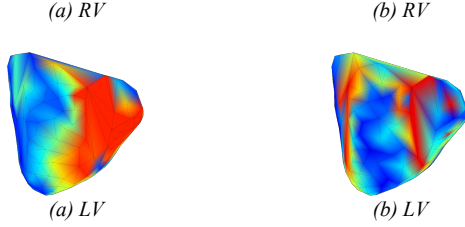
(a) LV　　　　　　　*(b) LV*

Figure 6. Angle (a) and speed (b) errors on the ventricles, performing CV1 on the reconstructed data.

4.　　Discussion

CV1 and CV2 gave comparable results for the simulated data (Table 1). However, for experimental data (Fig. 4), CV1 performed better than CV2. Nevertheless, the overall results are dependent on the customization of the local WF model. The model parameters are estimated at each electrode using neighbouring electrodes in order to reduce noise and imprecision. According to [1], the optimal number of neighbouring points is 20. However, in this study it is likely noise introduced by the inverse reconstruction on the estimation is not efficiently reduced, leading to poorly estimated model parameters and consequently an inaccurate velocity vector field. But, if the number of electrodes is increased, the local dimension of the estimation is lost. This suggests the results could be improved by reconstructing electrograms to higher-resolution meshes, before computing the velocity vectors.

The global outcomes are also dependant on the ECGi reconstruction quality and derivation of ATs. The high θ_{err} and s_{err} values (Fig. 5 & 6) are located at the onset and offset of activation. This corresponds to a known limitation of the ECGi technic. The torso volume smoothes high spatial frequencies of source distributions, leading to poor reconstruction of the pacing site [7]. In addition, high error values may be due to the far field activity dominating in region of low amplitude activation. Therefore, in these areas, the electrode of interest, and its neighbours have similar ATs, leading to an abnormally elevated estimated speed, and an inaccurate estimation of velocity. As well, high error values are located where confidence in the placement of the AT markers is low. Analysis of reconstructed speeds with respect to the gold standard reveals this. That is, the reconstructed speed is higher than the reference, *e.g.* for the simulated data with a pacing on the RV freewall, the gold standard gave a median speed of 0.77 m/s and 1.12 m/s for the reconstruction; For the experimental data with an epicardial pacing on the RV, the gold standard gave a median speed of 1.53 m/s and 3.39 m/s for the reconstruction. This increase of the overall estimated speed is due to a reduced AT dispersion, a known consequence of the inverse mapping [8]. Therefore, improvement of the ECGi reconstruction methods and the

ATs markers placing would improve cardiac CV estimation.

Nevertheless, the results show that the proposed CV mapping algorithm gives a good estimation of the propagation pattern (Fig. 3 and 4) with an overall median angle error less than 30°, suggesting this method could be useful in identifying sites of re-entry. Furthermore, although the estimated speed is not exact, regions of slow conduction may still be identifiable. The next step is to perform this algorithm on models with ischemia and scars. In these situations, CV2 will likely be more efficient due to the complexity of the cardiac propagation. In addition, the divergence and the curl of the velocity vector field [2] will be implemented to provide cardiac rhythm feature. Therefore, ectopic focal sources, zones of WF collisions and structural obstacles can be found.

5.　　Conclusion

In this paper, we proposed a method that assesses the WF velocity vectors from ECGi data. It relies on the spatial coordinates of reconstructed EGMs and theirs ATs and assumes either a locally linear or quadratic activation WF. The tool was performed on simulated and experimental data with no structural heart disease. For experimental data, CV1 gave better results and is more computationally efficient. Nevertheless, the main drawback of the method is the estimation of model parameters using inaccurate ATs that arise due to far field activity. Thus, an improvement of the non-invasive technique will create a better velocity vector estimation.

References

[1] Bayly PV, KenKnight BH, Rogers JM, Hillsley RE, Ideker RE, Smith WM. Estimation of Conduction Velocity Vector Fields from Epicardial Mapping Data. IEEE Trans on Biomed Eng 1998;45(5):563–71.

[2] Fitzgerald TN, Brooks DH, Triedman JK. Identification of Cardiac Rhythm Features by Mathematical Analysis of Vector Fields. IEEE Trans on Biomed Eng 2005;52(1):19–29.

[3] Ten Tusscher KHWJ. A Model for Human Ventricular Tissue. AJP Heart Circ Physiol 2003;286(4):H1573–89.

[4] Wang Y, Rudy Y. Application of the Method of Fundamental Solutions to Potential-based Inverse Electrocardiography. Ann Biomed Eng 2006;34(8):1272–88.

[5] Krause D, Potse M et al.. Hybrid Parallelization of a Large-Scale Heart Model. In: Keller R, Kramer D, Weiss J-P, editors. Facing the Multicore-Challenge II. Berlin: Springer; 2012:120–32.

[6] Bear LR, Cheng LK et al. The Forward Problem of Electrocardiography: Is it Solved? Circ Arrhythm Electrophysiol 2015;8:677–84.

[7] Schneider F, Dössel O, Müller M. Filtering characteristics of the Human Body and Reconstruction Limits in the Inverse Problem of Electrocardiography. Computers in

Cardiology 1998;25:689–92.

[8] Chengzong Han, Zhongming Liu, Xin Zhang, Pogwizd S, Bin He. Noninvasive Three-Dimensional Cardiac Activation Imaging From Body Surface Potential Maps: A Computational and Experimental Study on a Rabbit Model. IEEE Trans Med Imaging 2008;27(11):1622–30.

Address for correspondence.
Corentin Dallet, corentin.dallet@ihu-liryc.fr
IHU LIRYC, PTIB- Campus Hôpital Xavier Arnozan
Avenue du Haut-Lévèque, 33604 Pessac Cedex, France